Environmental Science and Pollution Research (2021) 28:3475–3483
https://doi.org/10.1007/s11356-020-10698-z

RESEARCH ARTICLE

Synthesis and characterization of Ni-doped anatase TiO_2 loaded on magnetic activated carbon for rapidly removing triphenylmethane dyes

Zhansheng Wu[1,2] · Xiufang He[2] · Zhenzhen Gao[1] · Yongtao Xue[2] · Xin Chen[2] · Luohong Zhang[1]

Received: 25 July 2020 / Accepted: 31 August 2020 / Published online: 12 September 2020

Abstract

In this work, we employed the in situ synthesis method to implant Fe_3O_4 into activated carbon (AC), in which the synthesis of the magnetic AC (MAC) was realized. Thence, Ni-doped anatase TiO_2 ($NATiO_2$) were anchored on different addition amount of MAC to synthesize the series of Ni-TiO_2/MAC photocatalysts. The chemical compositions and physical properties of these nanocomposites were analyzed by various characterization technologies. The photocatalytic capabilities of as-produced materials were then investigated via adsorption and photodegradation of triphenylmethane dyes (TPMs) as crystal violet (CV), basic fuchsine (BF), and malachite green (MG) solution. The results revealed that the removal of Ni-TiO_2/AC, Ni-TiO_2/2MAC, Ni-TiO_2/4MAC, and Ni-TiO_2/8MAC on TPMs is a very fast process and the removal efficiency can almost reach to about 90% in 10 min, and the catalyst has good cycle stability and is easy to be reused. This work provides a novel, low-cost, and effective way to rationally design and synthesize TiO_2-based photocatalysts for effective removal of TPMs.

Keywords Anatase TiO_2 · Magnetic activated carbon · Photodegradation · Triphenylmethane dyes

Introduction

Triphenylmethane dyes (TPMs), the third important dyes, have been widely employed in various fields, such as textile, leather, food, pharmaceutical, and cosmetic (Eich et al. 2020; Ye et al. 2019), which greatly satisfy people's life demands. However, the generation and release involved TPMs unspent during industrial production process or in the dying process, almost 15% or 280 kt in the whole world every year (Mishra and Maiti 2018). Since TPMs possessed complex aromatic structures, they cannot be destroyed completely, resulting in their gradual accumulation in the nature environment. Due to the properties of persistence in the environment and resistance to degradation, their mutagenic and carcinogenic properties are highly toxic to other living organisms and the environment (Gao et al. 2019). The conventional approach to mitigate dye problems are through the use of various physicochemical techniques based on precipitation, flocculation, redox processes, and electrochemical treatments (Bisht and Lal 2019; Kim et al. 2019; Saygili et al. 2019). However, these processes are not effective and generate large amount of toxic sludge as well as unable to degrade synthetic dyes drastically. Therefore, the complete removal of dyes has not been achieved. Thence, searching an efficient method to remove the dyes is urgent.

To address this challenge, many technologies towards wastewater treatment have been developed to remove the TPMs, including adsorption, biological progress, photocatalytic degradation, UV/H_2O_2, microwave-induced catalytic degradation, Fenton or Fenton-like processes, and electrochemical processes (Chen et al. 2019; Duman et al. 2016; Eskandarloo et al. 2016; Pei et al. 2016; Salveson et al. 2018). Then, developing a highly efficient method to remove the TPMs is an important research topic. Among these technologies, adsorption is recognized as one of the most efficient methods for its simple design and easy operation, while the photocatalytic degradation is regarded as an effective, feasible, and promising technology for its good stability, high activity, and strong oxidizability (Shi et al. 2018; Wu et al. 2020; Xue et al. 2019). However, there still existed some

Responsible editor: Santiago V. Luis

✉ Zhansheng Wu
wuzhans@126.com

✉ Luohong Zhang
1710501539@qq.com

[1] Xi'an Key Laboratory of Textile Chemical Engineering Auxiliaries, School of Environmental and Chemical Engineering, Xi'an Polytechnic University, Xi'an 710048, People's Republic of China

[2] School of Chemistry and Chemical Engineering, Shihezi University, Shihezi 832003, People's Republic of China

problems about the adsorption, such as difficult reclaim and the possibility of secondary pollution, while the lower contaminant gathered on the surface of the photocatalyst will lead to lower photodegradation efficiency. Therefore, developing an easy operation, simple reclaim, and highly efficient removal method attracted our attention. Inspired, we would composite a photocatalyst on activated carbon that can absorb a big amount of TPMs and then for rapidly photodegrading under the light irradiation, which can remove the TPMs efficiently.

Anatase TiO_2 (a-ATiO_2), a typical *n*-type semiconductors, has been widely employed in effectively removing many different kinds of harmful organic or inorganic contaminants own to its excellent photocatalytic activity, low cost, chemical inertness, and environmental friendliness (Ahadi et al. 2019; Low et al. 2019; Tu et al. 2017). However, anatase phase TiO_2 possesses large band gap of 3.2 eV, weak visible light response, and weak ability for the adsorption of contaminants and the difficulty of recycling and reusing nanometer-sized TiO_2 particles, limiting the use of a-TiO_2 (Li et al. 2016; Zou et al. 2016). To solve the problem, some researches have been proving that doping with various transition metal cations can lower the conduction band edge as well as extend the optical absorption of TiO_2-based systems to the visible light (Bramhankar et al. 2020; Liu et al. 2016). At the same time, it has been proved that TiO_2 with Ni doping can effectively decrease crystallite size, increase specific surface area, and reduce band gap of catalysts because the ionic radius of Ni^{2+} (0.72 Å) is similar to Ti^{4+} (0.68 Å) (Blanco-Vega et al. 2017; Lai et al. 2016; Robles-Aguila et al. 2014).

In addition, since the nano TiO_2-based photocatalyst dispersed in the polluted water, the recycling and reuse of nanocatalyst powder also retard the practical application (Yang et al. 2018; Zhu et al. 2020). Therefore, it is significant to find practical useful methods to overcome the obstacle of separation and recovery of TiO_2 catalyst particles from water. Generally, many researches have conducted to synthesize catalyst by introducing magnetic carriers (Fenoll et al. 2017; Lee et al. 2014; Nadimi et al. 2019). Through the introduction of magnetic carriers, the surface area of catalysts can be improved significantly because the agglomeration of nanocatalyst powders can be thus avoided, which are favorable for high photocatalytic performance, further enhancing the adsorption of toxic pollutants on catalyst composites (Zhu et al. 2020). Therefore, inspired by this, the nanocomposites that Ni-doped anatase TiO_2 loaded on magnetic activated carbon (MAC) were innovatively synthesized. And the composite was synthesized by Ni-doped TiO_2 regulated on the surface of MAC, via a simple and fast sol-gel method in this study. The fabricated catalysts were evaluated to various characterization techniques to acquire the information of structural and physical properties. The photocatalytic behavior of the as-prepared materials in the degradation of TPM contaminants under visible light irradiation at room temperature was conducted. Moreover, the effects of solution pH on the dye photodegradation system were also investigated. The probable mechanism of the photodegradation of TPM contaminants was probed. And the obtained nanocomposites can eliminate TPM contaminants from aqueous solutions effectively.

Materials and methods

Materials

TBOT (98.5%, Chengdu Kelong Chemical Reagent Factory), anhydrous alcohol (EtOH; Tianjin Fuyu Fine Chemical Co., Ltd.), and acetic acid (Tianjin Beilian Fine Chemical Development Co., Ltd.) were used. The activated carbon (AC) from wood was purchased from Henan Zhongbang Environment Protection Technologies Co., Ltd. $Ni(NO_3)_2 \cdot 6H_2O$ was purchased from Shanghai Macklin Biochemical Co., Ltd. Ferric chloride and ferrous sulfate and ammonia water (25%) were purchased from Tianjin Yongsheng Fine Chemical Co., Ltd. Crystal violet (CV), basic fuchsine (BF), and malachite green (MG) were purchased from Xi'an Chemical Reagent Factory. All these reagents were of analytical reagent grade. Deionized water was used throughout the experiments.

Preparation of nanocomposites

Synthesis of MAC

In a typical synthesis, an appropriate amount of $FeCl_3 \cdot 6H_2O$ and $FeSO_4 \cdot 7H_2O$ (molar ratio is 2:1) was dissolved in 40 mL of distilled water containing AC (where in Fe_3O_4/AC = 20, 40, and 80 wt%), ultrasonically dispersed for 30 min to form a brownish yellow solution, and then transferred to a 100 mL of three-necked flask, magnetically stirring at 65 °C for 1 h under N_2 atmosphere, and then 5 mL of ammonia water (25%) was slowly added into the reaction solution, kept stirred for 1 h, and then cooled to room temperature. After the sample was attracted to the bottom of flask by the magnetic attraction, the supernatant was decanted. The precipitate was repeatedly washed with deionized water and absolute ethanol until the pH of the solution was 7 and then dried for 12 h in an oven at 40 °C to obtain MAC particles, which were recorded as 2MAC, 4MAC, and 8MAC, respectively.

Synthesis of Ni-doped anatase TiO_2 nanoparticles

Tetrabutyl orthotitanate (TBOT) was used as a titanium source. Under stirring, 30 mL of TBOT was added to 65 mL of absolute ethanol, and the resulting solution was designated as solution A. Under continuous stirring, 14 mL of glacial acetic acid was dropwise added to 7 mL of distilled water containing 0.14 g of $Ni(NO_3)_2 \cdot 6H_2O$ (2 wt%), and the obtained solution was designated as solution B. Solution B was

dropwise added to solution A under constant stirring at room temperature and further stirred for 3 h. The acquired mixture was allowed to form a gel at room temperature, dried in an oven at 80 °C for 24 h, and then calcined at 500 °C for 3 h. The resulting sample was named Ni-TiO_2.

Synthesis of Ni-TiO_2/MAC nanocomposites

In brief, AC, 2MAC, 4MAC, and 8MAC were added to 100 mL of methanol, respectively, and then sonicated for 30 min, and an appropriate amount of Ni-TiO_2 was added to the solution (the mass ratio of AC or MAC to Ni-TiO_2 was 1:10) and further stirred for 24 h, and the methanol was evaporated and dried under vacuum at 40 °C for 24 h to obtain the nanocomposites. The obtained samples were recorded as Ni-TiO_2/AC, Ni-TiO_2/2MAC, Ni-TiO_2/4MAC, and Ni-TiO_2/8MAC, respectively.

Characterization of photocatalysts

X-ray diffraction (XRD) analysis was used to examine the crystal phase composition of the photocatalyst using a Rigaku Giegerflex D/Max B diffractometer (Rigaku Corporation, Tokyo, Japan) with Cu-Kα radiation (λ = 1.5418 Å) in the 2θ region of 20°–80° and scanning step of 0.02°. Transmission electronic microscopy (TEM) analysis was conducted using a microscope (Tecnai G2 F20, FEI, Hillsboro, Oregon, USA) at 100 kV. The N_2 adsorption and desorption isotherms at 77 K were acquired using a surface area analyzer (Micromeritics, ASAP-2020, Norcross, GA, USA). X-ray photoelectron spectroscopy (XPS) analysis of the obtained samples was performed (250XI ESCA, Thermo Fisher Scientific, Waltham, MA, USA) in the presence of Mg Kα X-ray source (1253.6 eV) under a vacuum pressure of < 10^{-6} Pa. The vibrating sample magnetometer (VSM) was adapted to acquire the hysteresis loop of catalysts.

Photocatalytic experiments

The photocatalytic capabilities of the synthesized catalysts were investigated by the degradation of CV, MG, and BF solution. A 500-W Xe lamp with a visible light filter (the light intensity is 1000 mw) was adapted as visible light source, and the distance between the reactor and lamp housing was set as 8.5 cm. The temperature of reactor was maintained at 25 ± 1.0 °C by using cooling water circulation throughout the entire photocatalytic system. Typically, 20 mg of the as-prepared catalysts was added to 50 mL of CV, BF, and MG solution (10 mg/L, pH = 7.0), respectively. Subsequently, the acquired reaction solution was stirred for 30 min in the dark until reaching the adsorption-desorption equilibrium before visible light illumination. The degradation experiment of each sample at different time intervals was examined. The samples were acquired at definite intervals after the reaction and immediately centrifuged at 8000 rpm for 10 min to remove catalyst particles for the analysis of the removal of TPM contaminants. CV, BF, and MG concentration in the supernatant liquid was conducted by a UV-5100 spectrophotometer at 592 nm (CV), 543 nm (BF), and 616 nm (MG), respectively. Removal efficiency (η) of the photocatalyst was calculated as follows:

$$\eta = \frac{C_0 - C_t}{C_0} \times \%$$

The apparent rate constant (K) of the samples was calculated as follows:

$$1n(C_t/C_0) = kt$$

where C_o and C_t are the concentrations of TPMs at the initial irradiation time and at a specific irradiation time [t (min)], respectively.

Radical scavenging experiments

The radical scavenging experiments were conducted to further elucidate the photocatalytic mechanisms of photocatalysts. Ammonium oxalate (AO) (h^+ scavenger), $K_2S_2O_8$ (e^- scavenger), tert-butanol (t-BuOH) (•OH scavenger), and p-benzoquinone (p-BQ) (•O_2^- scavenger) were added into the photodegradation reaction system to trap the holes (h^+), the electrons (e^-), hydroxyl radical (•OH), and superoxide radical (•O_2^-), respectively. In brief, 20 mg of as-produced photocatalyst and 10 mM of radical scavengers were added into 50 mL of 10 mg/L dye solution. And then, the suspension was irradiated under the same conditions of photocatalytic experiments. The removal efficiencies (η) of triphenylmethane dyes can be effectively calculated to determine the main role of active species in the dye removal process.

Results and discussion

X-ray diffraction

The XRD pattern of Ni-TiO_2/MAC, synthesized under identical conditions but with different contents of magnetic activated carbon, was presented in Fig. 1. The XRD pattern (shown in Fig. 1 (insert)) with intense peaks at approximately 20.8°, 23°, 26.6°, 29.0°, and 44.0° were ascribed to mesoporous activated carbon (Li et al. 2019). The displayed spectra match well with that of standard anatase TiO_2. (JCPDS 21-1272), and the samples all show the peaks located at 25.36°, 37.88°, 48.10°, 54.10°, 54.85°, and 62.81°, corresponding to the reflections of the 101, 004, 200, 105, 211, and 204 planes,

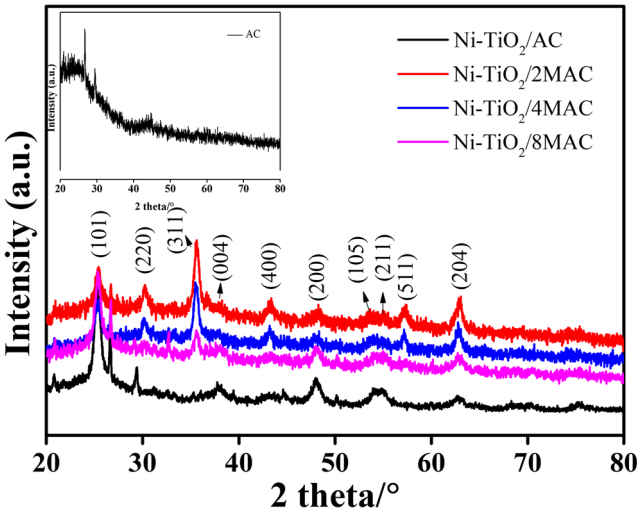

Fig. 1 XRD patterns of the Ni-TiO_2/AC, Ni-TiO_2/2MAC, Ni-TiO_2/4MAC, and Ni-TiO_2/8MAC and the AC sample (insert)

respectively (Chen et al. 2018; Ma and Wei 2020). Additionally, the XRD spectra of Fe_3O_4 implanted in activated carbon were also detected, located at about 30.15° (220), 35.63° (311), 43.25° (400), and 57.22° (511) (Karunakaran et al. 2014; Xi et al. 2011). Howbeit, peaks located at 53.8° (422) and 62.82° (440) were covered with the high-intensity peaks of anatase TiO_2 indicating that the Ni-TiO_2 is anchored on the magnetic activated carbon.

Transmission electronic microscope

The morphology and composition of the as-synthesized both Ni-TiO_2/AC and Ni-TiO_2/4MWAC were further revealed by TEM, HRTEM, and SAED techniques. The bright field patterns in Fig. 2a and 2b presented that inside the deeper place was the black Fe_3O_4 nanoparticles with uniform distribution and size; the edge of the shallower was the Ni-TiO_2, which indicated that Fe_3O_4 has been implanted in activated carbon and Ni-TiO_2 is evenly loaded on magnetic activated carbon (Cao et al. 2020; Karunakaran et al. 2014). The HRTEM image of Ni-TiO_2/4MWAC (Fig. 2c) manifested that the lattice fringe of 0.35 and 0.29 nm were ascribed to the 101 of anatase TiO_2 and the 220 of Fe_3O_4, respectively. As expected, concentric rings displayed in the SAED patterns support the nanocrystalline nature of the synthesized Ni-TiO_2/4MWAC.

N_2 adsorption-desorption

N_2 adsorption-desorption isotherms were measured to gain details about specific surface area and the pore size distributions of such structured Ni-doped anatase TiO_2 loaded on MAC materials, as depicted in Fig. 3 and Table 1. Notably, the isotherms of all products belonged to type IV isotherms with a distinct H_2 hysteresis loop in accordance with the IUPAC classification, indicating mesoporous characteristic,

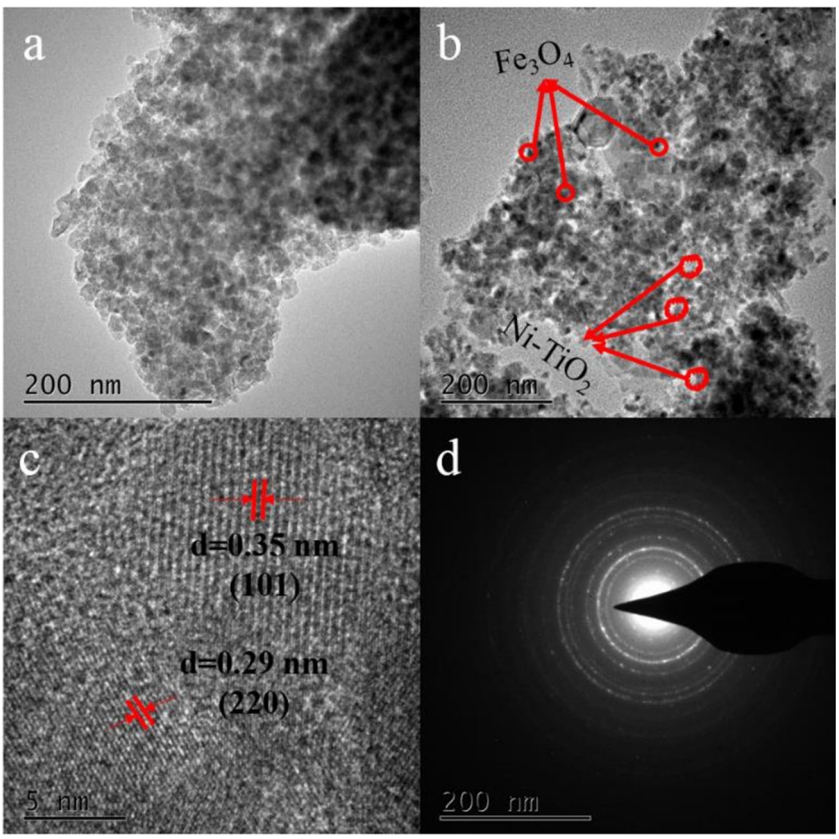

Fig. 2 TEM patterns of the (a) Ni-TiO_2/AC, (b) Ni-TiO_2/4MAC, (c) HRTEM image of the Ni-TiO_2/4MAC, (d) and SAED pattern of the Ni-TiO_2/4MAC

Table 1 BET parameters of the prepared materials

Photocatalysts	Specific surface area	Average pore size	Total pore volume
	(m^2/g)	(nm)	(cm^3/g)
Ni-TiO_2/AC	356.4	3.653	0.3254
Ni-TiO_2/2MAC	222.9	5.522	0.3077
Ni-TiO_2/4MAC	286.6	4.870	0.3489
Ni-TiO_2/8MAC	333.0	3.927	0.3267

which was consistent with the results of XRD characterization (Cao et al. 2020). Specifically, the specific surface areas of Ni-TiO_2/2MAC, Ni-TiO_2/4MAC, and Ni-TiO_2/8MAC were 222.9, 286.6, and 333.0 m^2/g, respectively, lower than Ni-TiO_2/AC (S_{BET} = 356.4 m^2/g). As shown in Fig. 3b, with an increasing content of Fe_3O_4, the content of pores distributed was about 3.7 nm. Combining the results, when the content of Fe_3O_4 increased, the pore structure of AC was not blocked. In other words, when the amount of Fe_3O_4 was high, the MAC is themed with Fe_3O_4 and AC was just wrapped on the surface of Fe_3O_4, which could indicate the Fe_3O_4-encapsulated AC structure (Karunakaran et al. 2014).

X-ray photoelectron spectroscopy

X-ray photoelectron spectroscopy (XPS) is a versatile surface analysis method that can be utilized to investigate the chemical states of the elements in Ni-TiO_2/4MAC with the results displayed in Fig. 4. It showed the XPS survey spectrum of Ni-TiO_2/4MAC sample (Fig. 4a). It can be seen that photoelectron lines at 284.8, 458.3, 530.4, and 710.9 eV corresponded to C 1s, Ti 2p, O 1s, and Fe 2p on the surface of the Ni-TiO_2/4MAC, respectively. As the Ni content was little for the samples, the Ni 2p peaks were not strong and hard to be found in Fig. 4a. In addition, there are strong signals of C and O for Ni-TiO_2/4MAC sample in the survey scan of XPS in Fig. 4a. Specifically, the strong C signal was attributed to the presence of AC. The high-resolution XPS spectrum of the Ti 2p, Fe 2p, Ni 2p, C 1s, and O 1s regions of Ni-TiO_2/4MAC was presented in Fig. 4b, c, d, e, and f. Specifically, in Fig. 4b, the binding energy at approximately 459.4 and 465.1 eV may be assigned to Ti 2p3/2 and Ti 2p1/2 in TiO_2, respectively, which is slightly higher than the pure TiO_2 (Ti 2p3/2 appears at 459.1 eV and Ti 2p1/2 at 465.0 eV). This further suggested that Ni has been successfully doped into the lattice of TiO_2 catalysts. Additionally, the difference between the two peaks was 5.7 eV, confirming the presence of Ti^{4+} in TiO_2 (Liu et al. 2017). As can be seen from Fig. 4c, the typical peaks at 710.9 and 724.8 eV are ascribed to Fe 2p3/2 and Fe 2p1/2 in Fe_3O_4, respectively, further demonstrating the formation of MAC (Yang et al. 2018). In Fig. 4d, the peak positions of Ni 2p3/2 and Ni 2p1/2 at 855.2 and 872.6 e V, respectively, with quite low signal-to-noise ratio due to the low Ni content, conform to the main chemical states of Ni in the samples which are Ni^{2+} (Yu et al. 2020). The high-resolution C 1s spectra (Fig. 4e) were fitted to the four peaks at around 284.8, 286.2, 287.4, and 288.8 eV and are consistent to C-C, C-O, C=O, and -COO (COOH), respectively. The O 1s high-resolution XPS spectra (depicted in Fig. 4f) are wide and asymmetric, suggesting there are at least two kinds of chemical states. The banding energies at 530.4 and 531.4 eV correspond to the crystal lattice oxygen (Ti-O-Ti) and chemisorbed oxygen (C-O), respectively.

Magnetic properties

The magnetic properties of the synthesized catalysts were evaluated by using a vibrating sample magnetometer (VSM), and the room temperature magnetic hysteresis loops for the Ni-TiO_2/AC, Ni-TiO_2/2MAC, Ni-TiO_2/4MAC, and Ni-TiO_2/8MAC were shown in Fig. 5. Additionally, the associated magnetic parameters such as coercive field H_c and

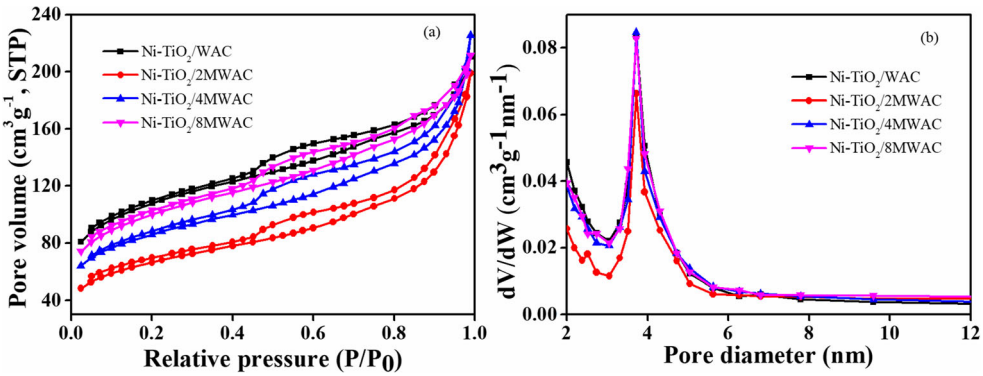

Fig. 3 N_2 adsorption-desorption isotherms (a) and pore size distributions (b) of samples

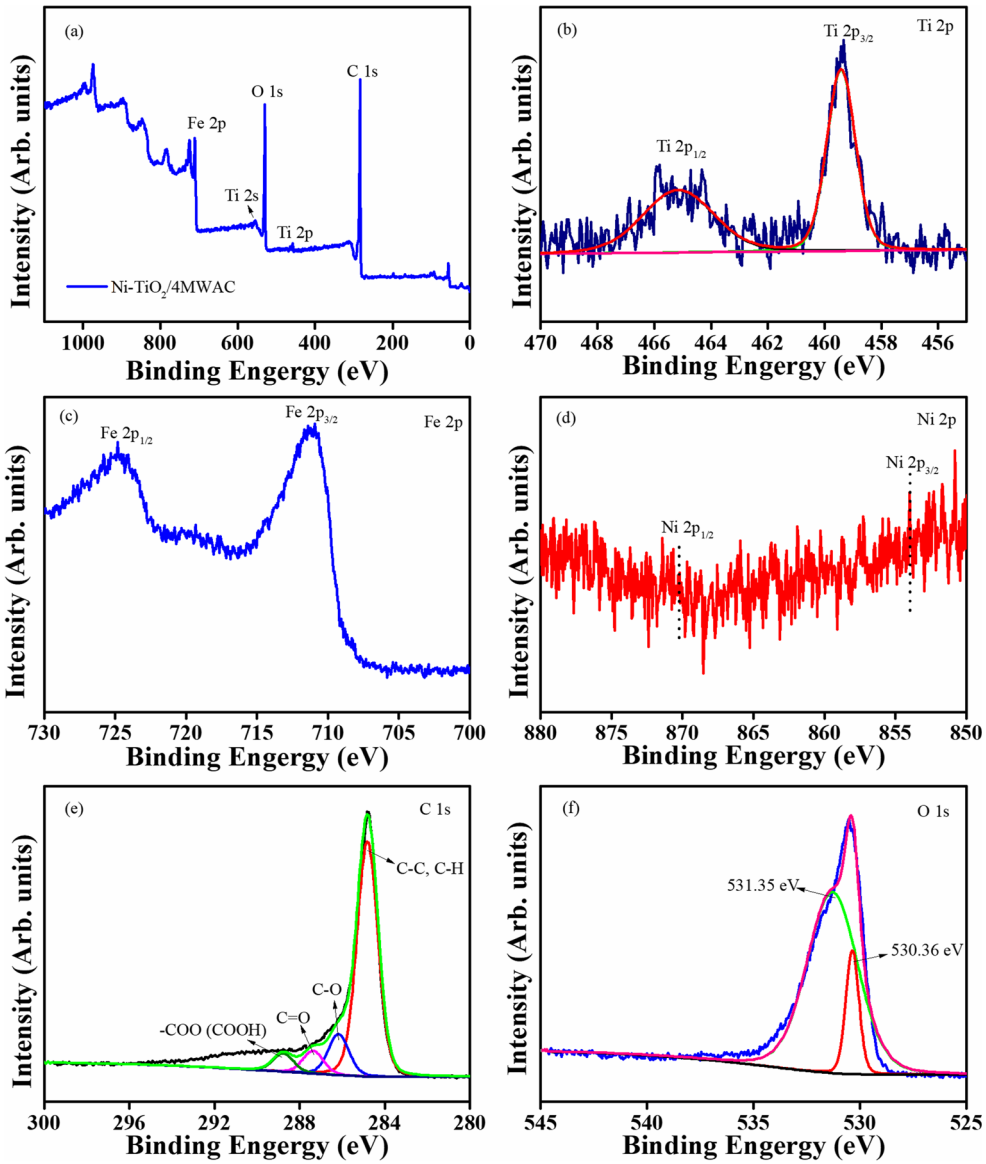

Fig. 4 The XPS survey spectrum (a) and high-resolution XPS spectra of Ti 2p (b), Fe 2p (c), Ni 2p (d), C 1s (e), and O 1s (f) on the surface of Ni-TiO_2/4MAC sample

saturation magnetization M_s showed that the Ni-TiO_2/2MAC, Ni-TiO_2/4MAC, and Ni-TiO_2/8MAC samples possessed similar magnetization hysteresis loops, and the M_s of samples with increasing Fe_3O_4 amounts slightly decreases, verifying

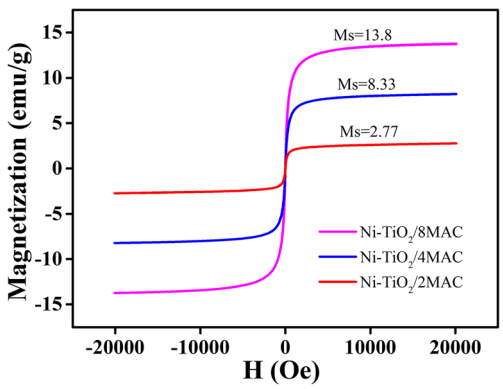

Fig. 5 The field-dependent magnetization curves of Ni-TiO_2/2MAC, Ni-TiO_2/4MAC, and Ni-TiO_2/8MAC at ambient temperature

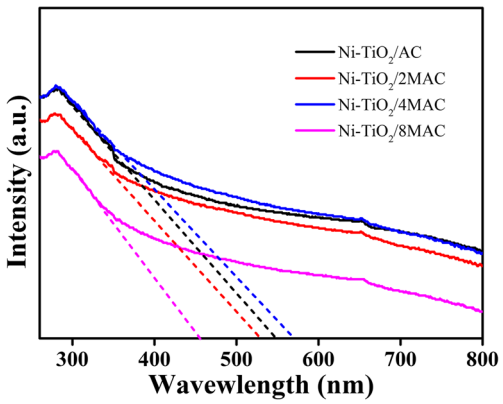

Fig. 6 The ultraviolet-visible spectra images of Ni-TiO_2/AC, Ni-TiO_2/2MAC, Ni-TiO_2/4MAC, and Ni-TiO_2/8MAC

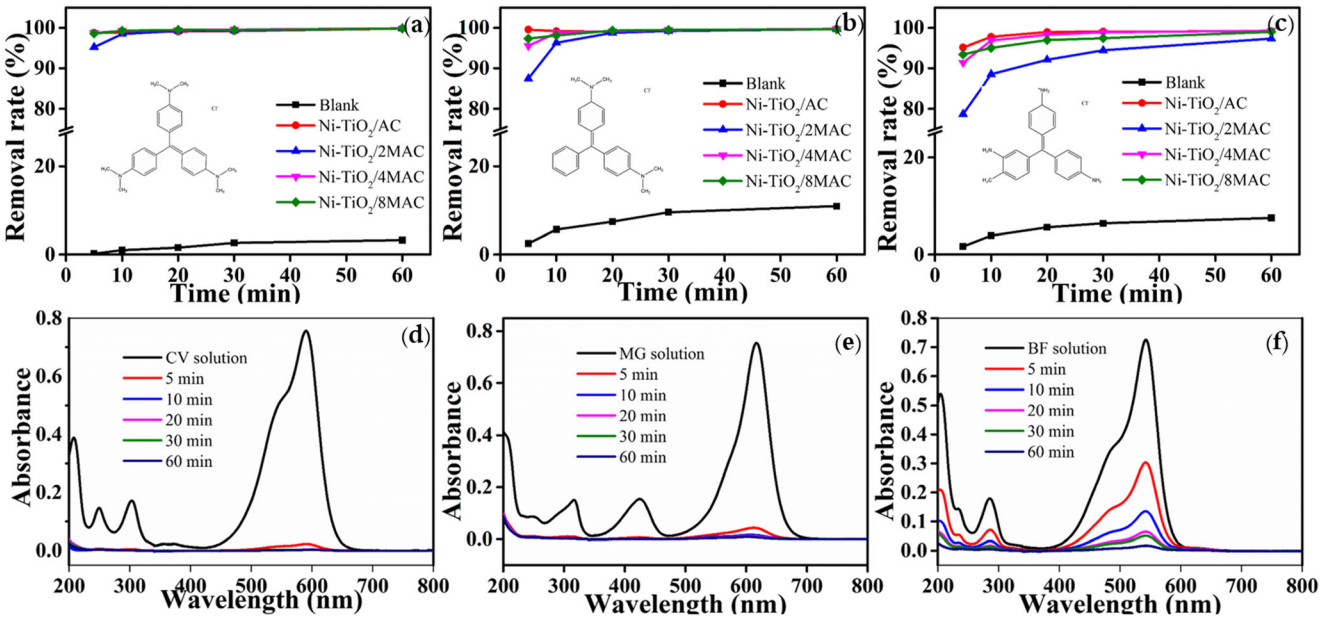

Fig. 7 The removal rate of dyes (CV (a), MG (b), BF (c)) by different photocatalysts and the full-wavelength scan pattern of CV (d), MG (e), and BF (f) on Ni-TiO_2/4MAC under visible light irradiation

the successful coating of Fe_3O_4 onto activated carbon (Fig. 5). The superparamagnetic behavior of the MACs makes it more easily separated by a magnet or a magnetic field. Meanwhile, the low M_r largely reduced the aggregation of MACs after it was separated magnetically from the original solution (Yang et al. 2018; Zhu et al. 2020).

UV-vis absorption spectra

To probe the light response property of the as-synthesized nanocomposites, the ultraviolet-visible absorption spectrometer (UV-vis) was adopted to acquire diffuse reflectance spectra images. It can be distinctly observed that the Ni-TiO_2/4MAC sample has the broadest absorption area; meanwhile, the absorption area of Ni-TiO_2/2MAC and Ni-TiO_2/4MAC is not markedly different from that of Ni-TiO_2/AC (Fig. 6). However, the Ni-TiO_2/8MAC has the smallest absorption area. This phenomenon could be explained by the absorption spectrum mainly composed of the overlapping absorption spectra of AC and Fe_3O_4, while the appropriate Fe_3O_4/AC ratio could have excellent light absorption performance (Karunakaran et al. 2014). Specifically, the band gap energies (Eg (eV)) of the products were estimated by the equation Eg = 1240/λg, where λg (nm) is the absorption wavelength threshold, and the Eg of Ni-TiO_2/AC, Ni-TiO_2/2MAC Ni-TiO_2/4MAC, and Ni-TiO_2/8MAC is 2.27, 2.35, 2.18, and 2.72 eV, respectively, indicating that a big amount of Fe_3O_4/AC may shelter the light adsorption, while a proper amount of AC and Fe_3O_4 may accelerate the light adsorption and the transfer of elections (Bai et al. 2017).

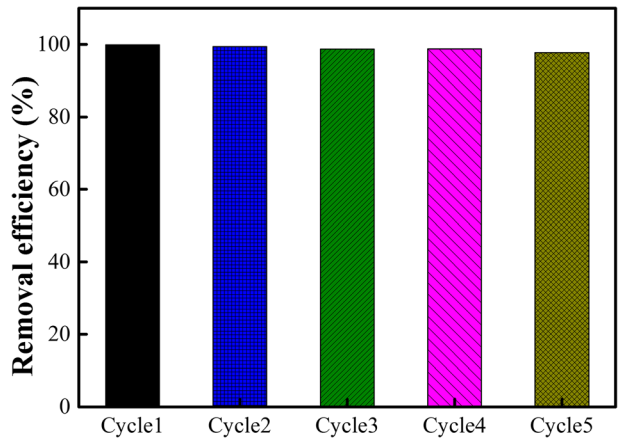

Fig. 8 Recycling of Ni-TiO_2/4MAC for CV removal

Photocatalytic performances and stability of photocatalysts

The photocatalytic performance of samples was evaluated for the photodegradation of TPMs under visible light irradiation. As depicted in Fig. 7, CV, MG, and BF were almost completely removed after 1 h of visible light irradiation over the Ni-doped anatase TiO_2 loaded on MAC photocatalysts. For comparison, within the first 10 min at 500-W visible light irradiation, the removal ratios of Ni-TiO_2/AC, Ni-TiO_2/2MAC, Ni-TiO_2/4MAC, and Ni-TiO_2/8MAC for CV are all as high as 98%. After the irradiation of 20 min, the removal ratio of TPMs by the materials was little changed. It can be attributed to the rapid consumption of active sites due to the rapid adsorption of the material.

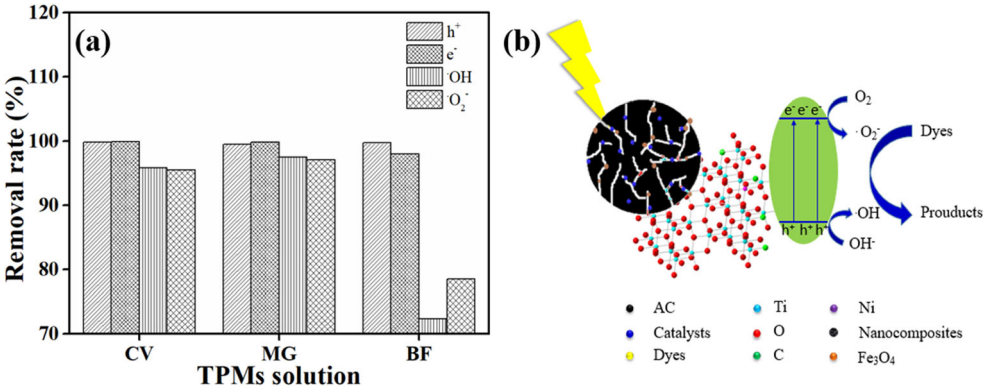

Fig. 9 The removal rate of CV, MG, and BF over Ni-TiO_2/4MAC in the presence of various radical scavengers (a) and the schematic of the proposed photocatalytic mechanism for TPMs on the Ni-TiO_2/4MAC photocatalyst under visible light irradiation (b)

Recycling experiment of Ni-TiO_2/4MAC for CV was conducted under visible light irradiation. The used Ni-TiO_2/4MAC was collected by centrifuge and then washed by deionized water and ethanol alternately for three times. Then, the collected Ni-TiO_2/4MAC was dried for use. The experiment was repeated for five times. The experimental results (Fig. 8) showed the removal efficiency of Ni-TiO_2/ 4 AC after five recycles, and the Ni-TiO_2/ 4 AC catalyst still has a good adsorption and degradation removal rate to CV solutions. Therefore, the Ni-TiO_2/ 4 AC catalyst has good cycle stability and is easy to be reused.

Photocatalytic degradation mechanism

In order to investigate the active substances in the photocatalytic degradation process, the results of free radical captured experiments are shown in Fig. 9a. The ·OH and $\cdot O_2^-$ values decrease significantly in the presence of radical scavengers, indicating that ·OH and $\cdot O_2^-$ play the major roles in the photodegradation of TPMs, especially in the degradation process of BF. The mechanism is shown in Fig. 9b. Since the TPMs can be adsorbed on the surface of AC in Ni-TiO_2/4MAC, a big amount of containment can be gathered on the surface of the Ni-TiO_2/4MAC. After the light is illuminated, a big amount of electron and hole pairs can be generated. Due to the introduction of Fe_3O_4, the electron can transfer from the interface of Ni-TiO_2 to that of Fe_3O_4 and then inhabit the recombination of electron and hole pairs, so a lot of ·OH and $\cdot O_2^-$ can be quickly generated, and then TPMs is degraded and finally decomposed into small molecules.

The main cause for the difference in degradation performance of Ni-doped anatase TiO_2 loaded on MAC materials is that when the content of Fe_3O_4 is low, the synergistic effect of Fe_3O_4 and AC could promote electron transfer between TiO_2 and MAC, which is beneficial to the photocatalytic process. In particular, the kinetics of degradation reached its peak when the content of Fe_3O_4 is 40% (Zhu et al. 2020). As the content of Fe_3O_4 increases gradually, the electron transfer pathway might transform to another way, which is the driving force to impel the TiO_2 and Fe_3O_4 forming the traditional type-I heterojunction (Karunakaran et al. 2014; Xi et al. 2011). Under this circumstance, it will reduce the redox performance of the whole catalyst, so the performance of Ni-TiO_2/8MAC is greatly cut down.

Conclusions

In summary, the activated carbon-supported Ni-doped anatase TiO_2 nanocomposite photocatalyst was prepared by introducing magnetic Fe_3O_4 nanoparticles. And the structure and physical properties of magnetic nanocomposites were analyzed by a series of characterization techniques. The Ni-TiO_2/AC catalyst and photocatalyst have a mesoporous structure, and the crystallite size of the composite materials is small, and the specific surface area and pore volume are slightly smaller than those of non-magnetic samples. The Ni-TiO_2/AC photocatalyst has a fast removal process and high removal rate for TPMs, and the free radical captured experiments indicated that ·OH and $\cdot O_2^-$ are the main active groups. This work provides a novel, low-cost, and effective way to rationally design and synthesize TiO_2-based photocatalysts to effectively remove TPM.

Funding This work was supported financially by funding from the National Natural Science Foundation of China (21868034) and the Shaanxi Provincial Key Research and Development Projects of China (2018KW-036).

References

Ahadi S, Moalej NS, Sheibani S (2019) Characteristics and photocatalytic behavior of Fe and Cu doped TiO_2 prepared by combined sol-gel and mechanical alloying. Solid State Sci 96:105975

Bai X, Li X, Gao Z, Hu Z, Hu G (2017) Novel fungal hyphae/Fe_3O_4 and N-TiO_2/NG composite for adsorption and photocatalysis. RSC Adv 7:6842–6848

Bisht V, Lal B (2019) Exploration of performance kinetics and mechanism of action of a potential novel bioflocculant BF-VB2 on clay and dye wastewater flocculation. Front Microbiol 10:1288

Blanco-Vega MP, Guzmán-Mar JL, Villanueva-Rodríguez M, Maya-Treviño L, Garza-Tovar LL, Hernández-Ramírez A, Hinojosa-Reyes L (2017) Photocatalytic elimination of bisphenol A under visible light using Ni-doped TiO_2 synthesized by microwave assisted sol-gel method. Mater Sci Semicond Process 71:275–282

Bramhankar TS, Pawar SS, Shaikh JS, Gunge VC, Beedri NI, Baviskar PK, Pathan HM, Patil PS, Kambale RC, Pawar RS (2020) Effect of

nickel–zinc co-doped TiO_2 blocking layer on performance of DSSCs. J Alloys Compd 817:152810

Cao Y, Zhou G, Zhou R, Wang C, Chi B, Wang Y, Hua C, Qiu J, Jin Y, Wu S (2020) Green synthesis of reusable multifunctional γ-Fe_2O_3/bentonite modified by doped TiO_2 hollow spherical nanocomposite for removal of BPA. Sci Total Environ 708:134669

Chen M, Ma J, Zhang B, Wang F, Li Y, Zhang C, He H (2018) Facet-dependent performance of anatase TiO_2 for photocatalytic oxidation of gaseous ammonia. Appl Catal, B 223:209–215

Chen SH, Cheow YL, Ng SL, Ting ASY (2019) Removal of triphenylmethane dyes in single-dye and dye-metal mixtures by live and dead cells of metal-tolerant *Penicillium simplicissimum*. Sep Sci Technol 54:1–11

Duman O, Tunç S, Bozoğlan BK, Polat TG (2016) Removal of triphenylmethane and reactive azo dyes from aqueous solution by magnetic carbon nanotube-κ-carrageenan-Fe_3O_4 nanocomposite. J Alloys Compd 687:370–383

Eich J, Bohm DA, Holzkamp D, Mankertz J (2020) Validation of a method for the determination of triphenylmethane dyes in trout and shrimp with superior extraction efficiency. Food Addit Contam, Part A 37(1):84–93

Eskandarloo H, Badiei A, Behnajady MA, Mohammadi Ziarani G (2016) Hybrid homogeneous and heterogeneous photocatalytic processes for removal of triphenylmethane dyes: artificial neural network modeling. CLEAN–Soil, Air, Water 44:809–817

Fenoll J, Garrido I, Pastor-Belda M, Campillo N, Viñas P, Yañez MJ, Vela N, Navarro S (2017) Solar detoxification of water polluted with fungicide residues using ZnO-coated magnetic particles. Chem Eng J 330:71–81

Gao Z, Wu Z, Chen X, Yang X (2019) Effective synthesis of nanoscale anatase TiO_2 single crystals using activated carbon template to enhance the photodegradation of crystal violet. Appl Organomet Chem 33:e4664

Karunakaran C, Vinayagamoorthy P, Jayabharathi J (2014) Nonquenching of charge carriers by Fe_3O_4 core in Fe_3O_4/ZnO nanosheet photocatalyst. Langmuir 30:15031–15039

Kim Y-W, Kim J-H, Moon DH, Shin H-J (2019) Adsorption and precipitation of anionic dye Reactive Red 120 from aqueous solution by aminopropyl functionalized magnesium phyllosilicate. Korean J Chem Eng 36:101–108

Lai L-L, Wen W, Wu J-M (2016) Ni-doped rutile TiO_2 nanoflowers: low-temperature solution synthesis and enhanced photocatalytic efficiency. RSC Adv 6:25511–25518

Lee HU, Lee G, Park JC, Lee Y-C, Lee SM, Son B, Park SY, Kim C, Lee S, Lee SC (2014) Efficient visible-light responsive TiO_2 nanoparticles incorporated magnetic carbon photocatalysts. Chem Eng J 240:91–98

Li D-N, Li J-N, Ma X-J (2019) Sustainable activated carbon hollow fibers from liquefied rubber wood (*Hevea brasiliensis*) and its adsorption of organic matter from solution. Wood Res 64:317–324

Li L, Chen Y, Jiao S, Fang Z, Liu X, Xu Y, Pang G, Feng S (2016) Synthesis, microstructure, and properties of black anatase and B phase TiO_2 nanoparticles. Mater Des 100:235–240

Liu DD, Wu ZS, Tian F, Ye B-C, Tong YB (2016) Synthesis of N and La co-doped TiO_2/AC photocatalyst by microwave irradiation for the photocatalytic degradation of naphthalene. J Alloys Compd 676: 489–498

Liu X, Xing Z, Zhang Y, Li Z, Wu X, Tan S, Yu X, Zhu Q, Zhou W (2017) Fabrication of 3D flower-like black N-TiO_2-x@ MoS_2 for unprecedented-high visible-light-driven photocatalytic performance. Appl Catal, B 201:119–127

Low J, Dai B, Tong T, Jiang C, Yu J (2019) In situ irradiated X-ray photoelectron spectroscopy investigation on a direct Z-scheme TiO_2/CdS composite film photocatalyst. Adv Mater 31:1802981

Ma C, Wei M (2020) $BiVO_4$-nanorod-decorated rutile/anatase TiO_2 nanofibers with enhanced photoelectrochemical performance. Mater Lett 259:126849

Mishra S, Maiti A (2018) The efficacy of bacterial species to decolourise reactive azo, anthroquinone and triphenylmethane dyes from wastewater: a review. Environ Sci Pollut Res 25:8286–8314

Nadimi M, Saravani AZ, Aroon MA, Pirbazari AE (2019) Photodegradation of methylene blue by a ternary magnetic TiO_2/Fe_3O_4/graphene oxide nanocomposite under visible light. Mater Chem Phys 225:464–474

Pei C, Han G, Zhao Y, Zhao H, Liu B, Cheng L, Yang H, Liu S (2016) Superior adsorption performance for triphenylmethane dyes on 3D architectures assembled by ZnO nanosheets as thin as ~1.5 nm. J Hazard Mater 318:732–741

Robles-Aguila MJ, Mendoza ME, Dávila-Jiménez MM, Bentrup U, Elizalde-González MP (2014) Influence of Ni doping on the structural, optical and textural properties of TiO_2 nanocrystals prepared via an ultrasound assisted sol-gel method. J Sol-Gel Sci Technol 69: 571–579

Salveson PJ, Haerianardakani S, Thuy-Boun A, Yoo S, Kreutzer AG, Demeler B, Nowick JS (2018) Repurposing triphenylmethane dyes to bind to trimers derived from Aβ. J Am Chem Soc 140:11745–11754

Saygili Y, Stojanovic M, Flores-Díaz N, Zakeeruddin SM, Vlachopoulos N, Grätzel M, Hagfeldt A (2019) Metal coordination complexes as redox mediators in regenerative dye-sensitized solar cells. Inorganics 7:30

Shi L, Ding W, Yang S, He Z, Liu S (2018) Rationally designed MoS_2/protonated g-C_3N_4 nanosheet composites as photocatalysts with an excellent synergistic effect toward photocatalytic degradation of organic pollutants. J Hazard Mater 347:431–441

Tu W, Li Y, Kuai L, Zhou Y, Xu Q, Li H, Wang X, Xiao M, Zou Z (2017) Construction of unique two-dimensional MoS_2-TiO_2 hybrid nanojunctions: MoS_2 as a promising cost-effective cocatalyst toward improved photocatalytic reduction of CO_2 to methanol. Nanoscale 9:9065–9070

Wu ZS, Xue YT, He XF, Li YF, Yang X, Wu ZL, Cravotto G (2020) Surfactants-assisted preparation of $BiVO_4$ with novel morphologies via microwave method and CdS decoration for enhanced photocatalytic properties. J Hazard Mater 387:1–11

Xi G, Yue B, Cao J, Ye J (2011) Fe_3O_4/WO_3 hierarchical core–shell structure: high-performance and recyclable visible-light photocatalysis. Chem Eur J 17:5145–5154

Xue YT, Wu ZS, He XF, Li Q, Yang X, Li L (2019) Hierarchical fabrication Z-scheme photocatalyst of $BiVO_4$ (040)-Ag@CdS for enhanced photocatalytic properties under simulated sunlight irradiation. J Colloid Interface Sci 548:293–302

Yang Z, Gong X-B, Peng L, Yang D, Liu Y (2018) ZnO-CNTs-Fe_3O_4 catalytic in situ generation of H_2O_2 for heterogeneous Fenton degradation of 4-chlorophenol. Chemosphere 208:665–673

Ye J, Jin L, Zhao X, Qian X, Dong M (2019) Superior adsorption performance of metal-organic-frameworks derived magnetic cobalt-embedded carbon microrods for triphenylmethane dyes. J Colloid Interface Sci 536:483–492

Yu H, Yang X, Wu Y, Guo Y, Li S, Lin W, Li X, Zheng J (2020) Bimetallic Ru-Ni/TiO_2 catalysts for hydrogenation of N-ethylcarbazole: role of TiO_2 crystal structure. J Energy Chem 40: 188–195

Zhu L, Kong X, Yang C, Ren B, Tang Q (2020) Fabrication and characterization of the magnetic separation photocatalyst C-TiO_2@ Fe_3O_4/AC with enhanced photocatalytic performance under visible light irradiation. J Hazard Mater 381:120910

Zou H, Song M, Yi F, Bian L, Liu P, Zhang S (2016) Simulated-sunlight-activated photocatalysis of methyl orange using carbon and lanthanum co-doped Bi_2O_3-TiO_2 composite. J Alloys Compd 680:54–59